16

Dual-Wavelength Pumped Dispersion-Compensating Fibre Raman Amplifiers

André Brückmann[1], Guido Boyen[1], Paul Urquhart[2], Amaia Legarrea Imízcoz[2], Nuria Miguel Zamora[2], Bruno Bristiel[3] and Juan Mir Pieras[3]
[1]*Hochschule Niederrhein*
[2]*Universidad Pública de Navarra*
[3]*Télécom Bretagne*
[1]*Germany*
[2]*Spain*
[3]*France*

1. Introduction

Fibre Raman amplifiers (FRAs) use optical pumping to provide low-noise gain in fibre waveguides by means of stimulated Raman scattering (SRS). They can be operated over a range of telecommunications windows, from below 1300 nm to beyond 1650 nm, often with broader spectra than those of erbium doped fibre amplifiers (EDFAs). The gain medium can be transmission fibre or dispersion compensating fibre (DCF). DCF-based Raman amplifiers simultaneously boost the propagating signals and compensate for accumulated chromatic dispersion, thereby fulfilling a dual role (Bromage, 2004, Urquhart et al., 2007).

Dispersion compensating Raman amplifiers (DCRAs) normally consist of modules incorporating several kilometres of DCF plus up to around twelve pumps at different wavelengths (Islam, 2004; Namiki et al., 2005), usually launched contra-directionally with respect to the signals, as illustrated in Fig. 1. The Raman gain is often several decibels above the transparency condition of the DCF medium to mitigate the loss of associated passive components. A single pump excites a gain profile with a full width at half height of ~7 GHz but it is far from spectrally uniform, rendering it unsuitable for wavelength division multiplexed (WDM) communications. Gain flattening is thus required and it is normally achieved by the multiple pumps. Complicated optical interactions occur within the fibre, in which power is coupled from the pumps to the signals, from one pump to another and from one signal to another. Additionally, there are the noise processes of amplified spontaneous Raman scattering and amplified distributed Rayleigh backscattering, which can be sufficiently powerful to contribute to the gain saturation. Nevertheless, by carefully optimising the launched powers, the desired spectral equalisation can be achieved.

Multi-wavelength pumped DCF modules have been used to provide gain bandwidths that exceed 100 nm with uniformities of better than 0.3 nm but they are complicated sub-systems (Giltrelli and Santagiustina, 2004; Namiki et al., 2004; Neto et al, 2009). Wavelength-stabilised pump lasers are expensive and the resulting gain spectra are sensitive to the precise values of the launched powers. Sophisticated simulation software with advanced

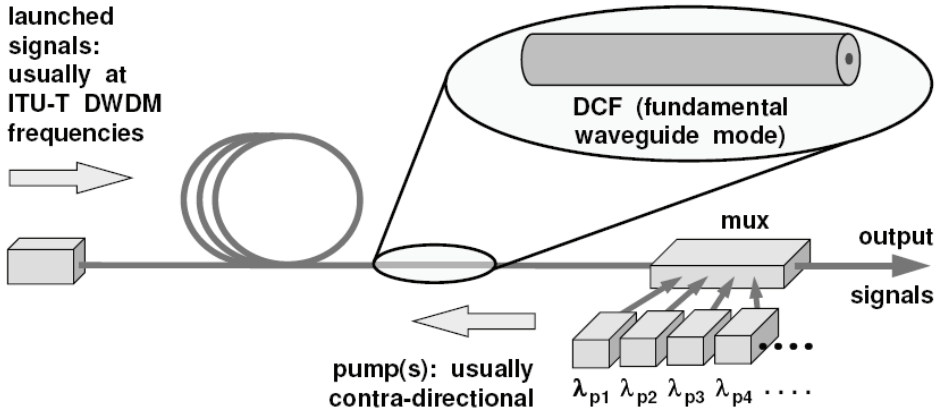

Fig. 1. Dispersion compensating fibre Raman amplifier with contra-directional multi-wavelength pumping. mux = pump-signal wavelength multiplexer.

optimisation algorithms is required to predict the best operating conditions. However, gain uniformity is perturbed by small changes in the power of any of the waves propagating in the fibre. Therefore, the possibility of, for example, the failure of a few channels, the addition of fibre splices elsewhere in the network or electrical power feed fluctuations to the pumps requires that there be continuous monitoring and re-optimisation.

The aim of this chapter is to present simulation results for a simpler and cheaper strategy for gain-equalised DCRAs and to understand its limitations. They are pumped with only two backward-propagating wavelengths (Koch et al., 1999) to obtain very broad spectra and then a customised gain equalising filter (GEF) provides profile uniformity comparable to the multi-wavelength strategy outlined above. Such amplifiers are relatively simple, offering application in cost-constrained networks, such as shorter regional links and in the metropolitan area, where large numbers of WDM channels are being deployed. We describe how they can amplify over 100 channels on the 100 GHz ITU-T dense WDM grid (ITU-T, 2002) with acceptable noise performance and achieve spectral equalisation of under 0.4 dB in typical operation. Moreover, they can tolerate growth in the number of channels, without necessarily having to change filter specifications. We have designed customised thin film transmission filters with spectral profiles specifically for this role and we explain their encouraging operational flexibility.

2. Overview of fibre Raman amplifiers

The SRS, upon which Raman amplification is based, is an inelastic scattering process, in which a pump wave, of frequency ν_p, surrenders energy to the medium through which it passes. The wave causes the medium's molecules to vibrate and any propagating signal at a lower frequency ν_s then receives energy from these excited molecules, producing additional photons at ν_s that are in phase with those of the signal; the result is amplification. An FRA can be provided, as shown in Fig. 1, by launching one or more pump waves into the same fibre as the signal(s). In this way, the signal(s) experience gain during transit in the fibre.

FRAs are "non-resonant"; in contrast to EDFAs, their operation does not depend on electronic energy levels. The non-resonant nature of SRS permits amplification over all

spectral regions where the fibre does not exhibit high loss, merely by the provision of one or more pump lasers of suitable wavelength and power. A single optical pump provides a gain profile that is characteristic of the fibre's glass constituents in the form of a spectrum of frequency shifts from ν_p to *lower* frequencies (i.e. longer wavelengths). The peak shift, which is material dependent, is commonly ~13 THz from ν_p. A profile for one reported DCF design is included in Fig. 2, from which a key feature for this chapter is evident: the gain is not at all spectrally uniform (Miyamoto et al., 2002; Namiki et al., 2005). The best pumping efficiencies are achieved by using fibre types with a small effective area (A_{eff}) to maximise the power concentration. This fact favours DCF as a Raman gain medium because in most designs A_{eff} is 15–25 μm², which is about a quarter of the value of many transmission fibres.

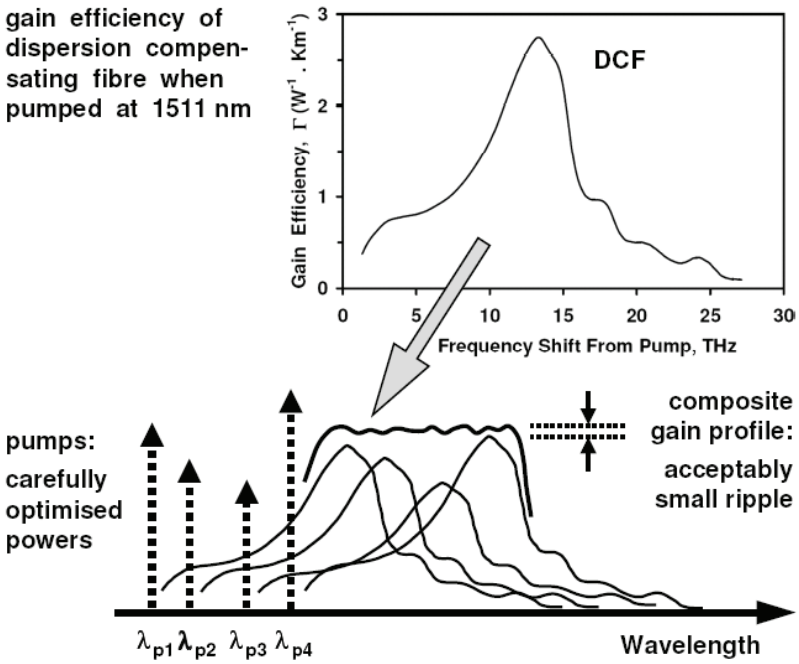

Fig. 2. Multi-wavelength pumping method of gain equalisation of a DCRA. The gain profile on the top right is adapted from Namiki et al., 2005. Other features are schematic.

Figure 2 shows how multi-wavelength pumping can provide spectral gain flattening. Every propagating pump contributes a gain profile and then a wide overall bandwidth of acceptable uniformity is obtained by launching several pumps of suitably optimised powers and wavelengths. However, as stated in Section 1, many interactions contribute to the amplification. Predicting the correct powers with only two pumps is reasonably straightforward using trial and error or by a simple systematic search procedure (as we have done). However, the effort becomes ever greater and the sensitivity to launched powers grows as the number of pumps is increased. Advanced optimisation algorithms are thus used to achieve gain flattening over a wide bandwidth (Cui et al., 2004; Miyamoto et al., 2002; Neto et al., 2009; Zhou et al., 2006).

Noise adversely affects all communications systems and in digital operation it increases the probability of bit errors (Urquhart, 2008). There are three main noise processes in FRAs: amplified spontaneous Raman scattering (often called amplified spontaneous emission, ASE), Rayleigh backscattering (RBS) and relative intensity noise (RIN) transfer. ASE is often the most prominent one and results from "spontaneous" Raman scattering, which occurs in a pumped fibre, irrespective of the presence of signal photons. Spontaneously scattered photons, which are created all along the fibre, encounter further excited (vibrating) molecules, caused by the presence of the pump, and they are amplified. The ASE power grows bi-directionally, sometimes reaching significant magnitudes with respect to the signal. It is broad bandwidth and unpolarised and it is transmitted to the detectors along with the signals, where it reduces the optical signal-to-noise ratio (SNR).

Rayleigh scattering results from microscopic random fluctuations in the glass's refractive index, which exist even in high quality fibres (Bromage et al., 2004; Jiang et al., 2007a). Variations that happen to be $\lambda/4$ for any of the guided waves provoke weak reflections that add in phase, creating a distributed reflector. The pump, signal and bi-directional ASE waves are all reflected but, unlike SRS, the process is "elastic" and so there are *no* frequency shifts. Rayleigh scattered waves are themselves reflected, causing double scattering. As the backscattered waves progress in the fibre they experience amplification, due to the presence of pump photons, becoming reasonably powerful. RBS enhances the ASE power and it causes time-delayed replicas of the signals to be incident on the detectors. In either case, the consequence is a reduction of the SNR.

Normally, the pump lasers are continuous wave but, owing to the oscillatory interactions within their semiconductor active media, they always exhibit random high frequency temporal power fluctuations, known as RIN. Raman gain occurs within a silicate fibre on a sub-picosecond time scale and so it is almost instantaneous. Consequently, when the pumps and signals travel in the same direction in the fibre, the random fluctuations of the pumps are directly transferred to the signals and the effect is amplified within the gain medium. Fortunately, there is a simple means to reduce the problem significantly, which is contra-directional pumping, as shown in Fig. 1. The waves then pass through each other, providing good time averaging during transit. Throughout this chapter, we assume the use of such pump schemes and so RIN transfer is ignored in our analysis.

3. Theory

The optical fibre gain medium, such as in Fig. 1, has a length coordinate z, which ranges from 0, at the signal input, to L, at the pump launch point. It is specified by a Raman material gain coefficient, g ($W.m^{-1}$), an effective area, A_{eff} (m^2), a loss coefficient, α (m^{-1}) and a Rayleigh scattering coefficient γ (m^{-1}). All of these parameters depend on the fibre's glass composition and waveguide design and they vary with wavelength (Jiang et al., 2007b). When modelling FRAs it is convenient to define a gain efficiency, Γ ($W^{-1} \cdot km^{-1}$) for any two interacting frequencies ν_i and ν_j (corresponding to wavelengths λ_i and λ_j):

$$\Gamma(\nu_i, \nu_j) = g_{i,j} / K A_{eff} \; ; \; \nu_i < \nu_j \tag{1}$$

The constant K accounts for the polarisation states of the two interacting waves and in most circumstances, where there is good randomisation, K = 2. A plot of Γ, which applies when λ_p is 1511 nm (Namiki et al., 2005), is included in Fig. 2. The values presented can be scaled for

another *pump* wavelength, $\lambda_{p\text{-}new}$ in nm, using $\Gamma(\lambda_{p\text{-}new}) = (\lambda_{p\text{-}new}/1511)\,\Gamma$. Plots of $\alpha(\lambda)$ and $\gamma(\lambda)$ for the same DCF type are also presented by Namiki and Emori, 2005.

The signal and pump waves enter the amplifier at z = 0 and z = L, respectively and broad band bi-directional ASE grows throughout the fibre. Raman interactions occur between any pair of guided waves (be they pump, signal or ASE) regardless of their wavelengths, direction of propagation or whether they are modulated to vary in time. Power transfer is from the higher frequency (shorter wavelength) waves to the lower frequency (longer wavelength) ones. Moreover, all guided waves are subject to both loss and RBS. The amplifier is modelled by establishing sets of bi-directional differential equations to account for all of these influences.

The format that we use in Sections 5 – 8 is stated in Equation (2), the derivation of which is outside the scope of this chapter, but details are in Agrawal, 2005 and Islam et al., 2004.

$$\begin{aligned}\pm\frac{dP_i^{\pm}}{dz} \;=\; & +P_i^{\pm}\sum_{j=1}^{i-1}\Gamma(\nu_j,\nu_i)\cdot P_j \;+\; p_{0i}\sum_{j=1}^{i-1}\Gamma(\nu_j,\nu_i)\cdot P_j\cdot H(\nu_j-\nu_i)\\ & -P_i^{\pm}\sum_{j=i+1}^{N}(\nu_i/\nu_j)\cdot\Gamma(\nu_j,\nu_i)\cdot P_j \;-P_i^{\pm}\sum_{j=i+1}^{N}(\nu_i/\nu_j)\cdot\Gamma(\nu_i,\nu_j)\cdot 2p_{0j}\cdot H(\nu_i-\nu_j)\\ & -\alpha(\nu_i)P_i^{\pm}+\gamma(\nu_i)P_i^{\mp}\;,\end{aligned}\qquad(2)$$

where $P_{i,j} = [\,P_j^{+} + P_j^{-}\,]$. Equation (2) describes the evolution of all of the propagating waves: the pumps, the signals plus a segmentation of the bidirectional ASE into N bands of width $\Delta\nu$ that are sufficiently narrow to provide realistic spectral resolution but not so numerous as to create excessive computation. The length-independent terms $p_{0i,j}$ are the "spontaneous scattering equivalent input powers", given by $p_{0i,j} = 2h\nu_{i,j}\,\Delta\nu$, where h is Planck's constant and the factor of 2 accounts for the fibre's orthogonal polarisation modes. The factor of 2 within the fourth term on the right of Equation (2) results from the two directions of the ASE. The function H, called the "ASE thermal factor" or "Bose-Einstein factor", quantifies the temperature variation of the spontaneous scattering, (Lewis et al., 1999):

$$H(\nu_j-\nu_i) \;=\; 1 \;+\; \{\exp[\,h\cdot(\nu_j-\nu_i)/k_B T\,] - 1\}^{-1}\,,\qquad(3)$$

where k_B is the Boltzman constant and T is the temperature (Kelvin).

The amplifier's "net" (or "input-output") gain, G_{net} is specified as the ratio of signal powers at one of the channel wavelengths, $G_{net} = P(\lambda_s, z = L)/P(\lambda_s, z = 0)$, and it is converted to decibels when necessary. Another definition, the "on-off" gain, is important for distributed amplification (Urquhart, 2008) but it is not used here. Equation (2) is a comprehensive model, incorporating many phenomena, at the cost of sacrificing physical insight. With this limitation in mind, we have derived an approximate analytical formula for dual wavelength pumping and it is stated as an appendix in Section 11.

The noise performance of an optical amplifier is specified by its "noise figure" (NF), which should be minimised when other considerations, such as cost, permit. When regarded as a black box, Raman (or other phase-insensitive) amplifiers exert three main influences: they amplify the signal(s), amplify the incident noise and add noise of their own. The NF quantifies the amplifier's deterioration of the optical SNR. It is the ratio of the optical SNR at input and output of the amplifier, as measured within a *narrow* optical bandwidth $\Delta\nu$, and the format that we use is:

$$NF = \frac{1}{G_{net}}\left(1 + \frac{P^{+}_{ASE}}{h\nu_s \Delta\nu} + \frac{P^{+}_{RBS}}{h\nu_s B}\right) \quad (4)$$

P^{+}_{ASE} is the forward propagating ASE power within $\Delta\nu$, imposed by a filter at the detector that is centred on signal frequency ν_s. P^{+}_{RBS} is the Rayleigh backscattered power incident on the detector within a bandwidth B (in Hz) defined by an *electrical* filter. Care is required to account for the states of polarisation in the RBS contribution; Bromage et al., 2004 explains the need for a factor of 5/9 in the equations. The literature on distributed Raman amplifiers often refers to an "effective noise figure" (Agrawal, 2005) but it is not used here.

Amplifiers are commonly concatenated or used together with loss elements, such as passive spans of fibre and optical components. Their total noise figure can be determined from the "Friis cascade formula" (Desurvire, 1994). For two elements with net gains G_1 and G_2, having noise figures NF_1 and NF_2, respectively,

$$NF_{total} = NF_1 + (NF_2 - 1)/G_1 \ , \quad (5)$$

where all terms are linear (*not* decibel) quantities. A passive loss element can be assigned a "gain" in the range $0 < G_{loss} < 1$ but it produces neither ASE nor significant RBS noise. Thus, by Equation (4), it has a noise figure of $1/G_{loss}$, which is greater than unity. A key property of Equation (5) is that it is non-commutative; the order of its constituents matters. The total noise figure for a loss element that precedes an FRA is $NF_{total} = NF_{FRA}/G_{loss}$. In contrast, if the loss follows the FRA, Equation (5) gives $NF_{total} = NF_{FRA} + (1 - G_{loss})/(G_{loss} \cdot G_{FRA})$. Substitution of some typical values, such as $G_{loss} = ½$, $G_{FRA} = 10$ and $NF_{FRA} = 6$, reveals that the lowest total noise figure is obtained by placing the passive loss *after* the fibre Raman amplifier. A loss element in front of it attenuates the signal plus any input noise. Thereafter, the amplifier provides gain and (importantly) it adds noise in the process. However, if the loss follows the amplifier, the amplified signal plus the added noise are attenuated equally by the loss element. For this reason, the GEF and associated components that we consider are located after the amplifying fibre, further details of which are in Section 4.

Guided waves in optical fibres are subject to nonlinear optical interactions, such as self-phase modulation, cross-phase modulation and four-wave mixing, all of which increase the bit error rate. Normally the effects are not problematical in a few kilometres of fibre but DCFs have small core diameters and high germania-content glasses, both of which enhance the nonlinear optical processes (Boskovic et al., 1996). Moreover, the Raman gain maintains a higher signal power along the fibre, which is also detrimental in this respect. The key effects that cause nonlinear crosstalk in optical systems all depend on a nonlinear phase shift, which is determined by a path-averaged power at each signal wavelength λ_s:

$$\Phi_{NL}(\lambda_s) = \frac{2\pi n_2}{\lambda_s A_{eff}} \int_{z=0}^{L} P_s^{+}(z) \cdot dz \ , \quad (6)$$

where n_2 is the nonlinear refractive index ($m^2.W^{-1}$) of the core of the DCF. A typical value of the ratio n_2/A_{eff} for DCF is 1.55×10^{-9} W^{-1}, which is higher than for standard single mode transmission fibre, mainly due to the difference in effective areas. The value of Φ_{NL} (radians) should be as low as possible and so it provides a means to compare FRAs in different operating regimes. Equation (6) is used in Section 8 in this comparative manner.

4. Gain spectrum equalisation

Our simple method to obtain gain equalisation is illustrated in Fig. 3, in which there are only two pumps plus a customised GEF. The filter is electrically passive, requiring neither power feeds nor control circuits. It is placed after the DCF to minimise the impact on the overall noise figure and lessen the disruption in the event of post-installation upgrades. The optical isolator prevents reflections from the GEF re-entering the amplifier and causing multipath interference noise. The two pumps provide a straightforward means to obtain a broad composite gain profile that has two peaks with a central minimum between them. We refer to the gain at this central minimum as the "baseline". The GEF is then designed to suppress the gain above the baseline by presenting a wavelength-dependent passive loss, as shown in Fig. 3. Thus the filter's transfer function, T(λ) is the inverse of the gain curve above the baseline. The gains are in decibels but T(λ) is linear:

$$G_{\text{baseline}}^{(\text{dB})}(\lambda) \;=\; T(\lambda)\cdot G_{\text{DCF}}^{(\text{dB})}(\lambda)\,, \tag{7}$$

The GFFs that we simulate are thin film interference filters, composed of alternating layers of high and low refractive index dielectrics deposited on a transparent substrate (Macleod, 2010). Two favoured vitreous film materials for operation in the S-, C- and L- bands are silica (SiO_2) and tantalum pentoxide (Ta_2O_5), which have refractive indices at 1550 nm of ~1.465 and ~2.065, respectively. We assume a substrate refractive index of 1.55 and that the entry medium is air. Thin film filters are a versatile and mature technology with dependable design and fabrication methodologies that allow excellent quality control and good production yields. Low cost and robust packaging is available with single mode fibre pigtails and low insertion losses. Moreover, thin films are one of the most thermally insensitive filter types, making them ideal for outdoor applications (Takahishi, 1995).

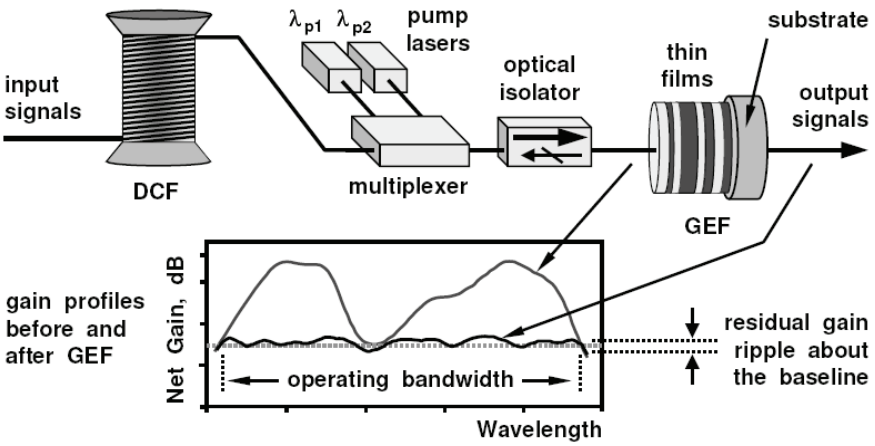

Fig. 3. The use of a passive thin film gain equalisation filter (GEF) to provide spectral flattening of a dual-wavelength pumped dispersion compensating fibre Raman amplifier. The thin film structure is not to scale and is shown unpackaged.

Light incident on the boundary between two films encounters a refractive index discontinuity, causing partial transmission and partial reflection. It also undergoes thickness and refractive index dependent phase changes in transmitting within each film. Filter simulation normally uses a matrix methodology with complex electric fields to account for the infinite number of coherent superpositions that occur during transit through a multi-layer film stack. The end result is a filter transfer function, normally expressed as the wavelength variation of the transmittance, T(λ), the *real* function used in Equation (7).

The matrix formulation of thin film optics predicts T(λ) for a user-defined film stack but it does not do the opposite and specify the stack structure to create a user-defined T(λ). For that we need to supplement the matrix calculations with an optimisation procedure. The approach that we used is called the "needle method" (Tikhonravov et al., 1966; Sullivan and Dobrowolski, 1996; Thelen et al., 2001), which is a numerical technique that inserts a small needle into an empty or a given starting structure. The needle is a layer of a refractive index which is lower than that of the surrounding material. After its insertion, a merit function is calculated and the algorithm changes the position of the needle. (The merit function is commonly a root mean square difference between the target value of T(λ) and the value obtained.) The algorithm repeats the needle placement until all positions have been evaluated and it then fixes the needle at the one with the lowest merit value. Many needles must be inserted until an acceptable design is found. Often a needle is placed adjacent to another one, which indicates that the thickness of the existing needle is insufficient and that a thicker layer yields a better merit value. Some implementations combine those needles into one layer; others refine the thicknesses after every insertion.

We performed the algorithm by using needles of different thickness to achieve an almost refined result at the end of each insertion step. This is a simple approach which achieves *desirable* sub-optimal designs. Takashashi, 1995 explains how sub-optimal designs of thin film filters are less sensitive to fabrication errors and temperature fluctuations. Depending on the accuracy chosen for incrementing the thickness and position, there are k calculations for the thickness and for each thickness there are m calculations for every position. We therefore had to compute $k \cdot m$ merit values for each needle, which can be very time consuming. However, because all of these calculations were based on the same TFF structure, we could subdivide them into small packets of parameters that were distributed to many computers, allowing us to reduce the time to obtain a result and/or to use a smaller step size to find a more optimised TFF. Nevertheless, even with a network of 20 standard desktop PCs, each synthesis could take several days of run time.

It is instructive to contrast the computer processing requirements of the two gain equalisation strategies: multiple pumps (Fig. 1) or dual pumps plus a static GEF (Fig. 3). Multi-wavelength pumping imposes more demanding pump power optimisation, which can be in real time to adapt to revised network requirements. In the GEF strategy the heavy computation is performed during the filter's development but it is not in real time. After GEF installation, any adjustment of the amplifier's pumps is relatively straightforward because there are only two to control. (Our approximate analytical model in Section 11 provides an insight into this aspect.) In effect, the computational burden is thus shifted from amplifier operation to the GEF production. A comparison of the two strategies is outside the scope of this chapter. However, a key consideration is the flexibility to adapt to changing amplifier operating requirements: does a sub-optimal filter synthesis leave sufficient latitude for network upgrading? This theme is addressed Sections 6 and 7.

5. Small signal and saturation regimes with a GEF

We start by simulating the net gain form 10 km of DCF and the results are plotted in Fig. 4. DCF spans are determined primarily by the transmission system's chromatic dispersion (Grüner-Nielsen et al., 2006). Our choice of 10 km is slightly longer than usual to provide pessimistic values of unpumped losses and a more challenging gain profile to flatten. The (contra-directional) pumps were at λ_{p1} = 1435 nm and λ_{p2} = 1485 nm to provide amplification across all of the communications C-band plus parts of the S- and L- bands.
In order to obtain small signal behaviour, we launched 151 channels separated by 100 GHz (over an extension of the ITU-T DWDM grid) with powers of -35 dBm per channel. Our total launched signal power was therefore 47.8 μW and the resulting signal wavelength range was between 1490 and 1611 nm. The 115 exiting channels from 1514 to 1606 nm are plotted as Curve a on Fig. 4. The pump powers, specified in Table 1, were chosen to ensure two peaks of equal magnitude and a minimum between them that is as close as possible to 3 dB, which was our selected baseline gain. The difference between the baseline and the gain peaks is the "excursion" and in Curve a it is 2.93 dB, which applies at ~1534 nm and ~1590 nm. We chose a baseline of 3 dB as it would be useful to overcome additional losses of associated components, such as the multiplexer and isolator shown in Fig. 3. Alternatively, suitably selected pump powers enable other values, as addressed in Section 7. The analytical model that we report in Section 11 gives further insight into the small signal limit.
We turn to saturated operation. In Curve b in Fig. 4 we used the same pump powers as in the small signal simulation but we launched 115 signals with the higher powers of -3 dBm/channel, causing two main effects: pump depletion and signal-to-signal Raman

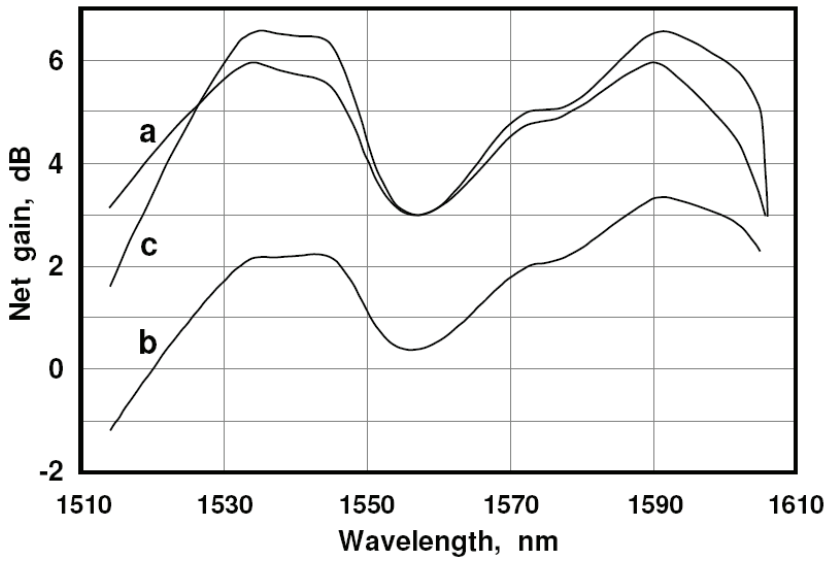

Fig. 4. Gain spectra for a dual-wavelength pumped DCF of length L = 10 km. Curve a: small signal operation, 151 channels with – 35 dBm/channel (but only 115 of them are plotted). Curves b and c: 115 channels spaced 100 GHz with –3 dBm/channel. The pump powers are stated in Table 1.

Operating mode	Channel power, dBm	Power λ_{1435}, mW	Power λ_{1485}, mW
Small signal	-35	173.3	89.1
Saturating signal, no pump readjustment	-3	173.3	89.1
Saturating signal with pump readjustment	-3	373.2	129.3

Table 1. Pump powers for different operation modes for Figs. 4 and 5.

interactions. Consequently, the gains are lower and there is an overall tilt, the most obvious manifestation of which is that the long wavelength peak is higher than the short wavelength peak. Curve c of Fig. 4 also uses 115 saturating signals of -3 dBm/channel but the pump powers have been readjusted to ensure two equal peaks and a central minimum of 3 dB. As stated in Table 1, higher pump powers were required to achieve this condition. In Curve c the operating bandwidth is about 88 nm and the gain excursion is now 3.56 dB.

The amplifier's noise figures are plotted in Fig. 5, where the curves correspond directly to those of Fig. 4. Small signal operation provides the lowest NF, followed by the saturating signals with unadjusted pump powers, followed by the saturated signals with readjusted pump powers. All curves show higher values at shorter wavelengths, which results mainly from the thermal factor that influences the ASE spectrum. In general, the NF depends on the signal and pump powers plus the powers of any other propagating waves, such as the ASE and Rayleigh scattering, within the fibre gain profiles. In common with EDFAs and other amplifier types, lower signal and ASE powers cause light or negligible saturation and lower noise figures. There are two peaks on Curve c associated with the two gain peaks on Fig. 4. By re-performing the calculation with $\gamma(\lambda) = 0$ to eliminate all distributed reflections, we have found that they are caused largely by Rayleigh backscattering of the signals and ASE.

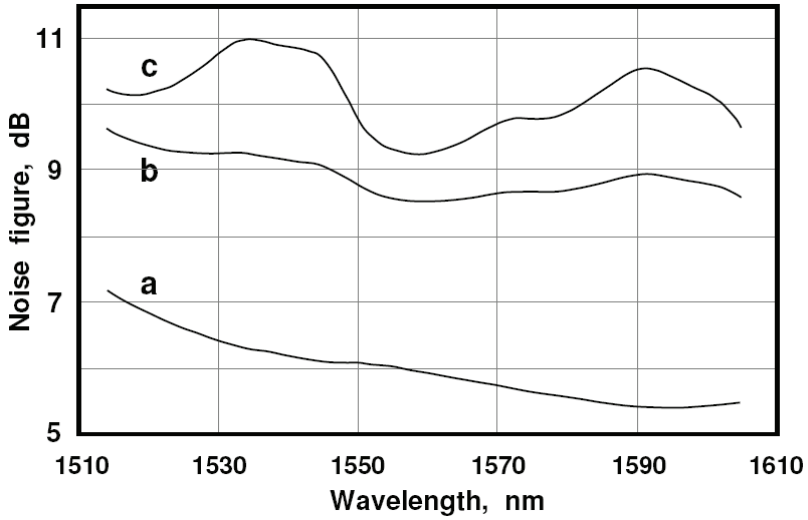

Fig. 5. Noise figure spectra for a dual-wavelength pumped DCF of length L = 10 km. Curve a: small signal operation, 151 channels with –35 dBm/channel (but only 115 of them are plotted). Curves b and c: 115 channels spaced 100 GHz with –3 dBm/channel. The pump powers are stated in Table 1.

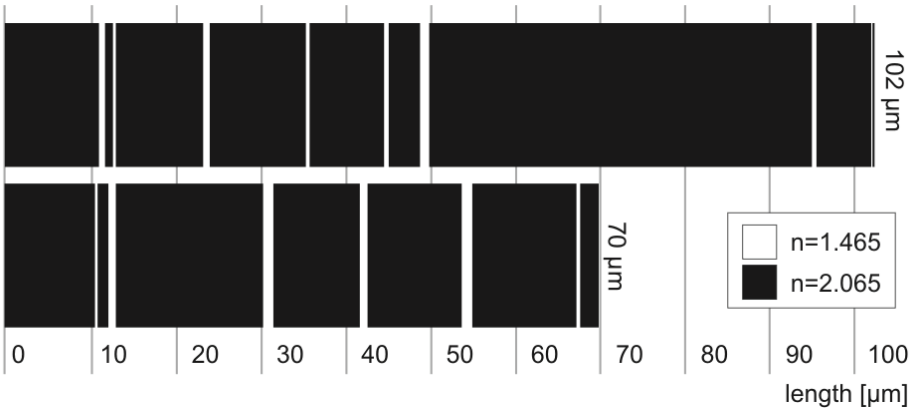

Fig. 6. Thin film structures formed from layers of SiO_2 (refractive index 1.465) in Ta_2O_5 (refractive index 2.065). Top: fifteen-layer filter to flatten Curve a in Fig. 4. Bottom: fourteen-layer filter to flatten Curve c in Fig. 4. The finer layers are not easily seen.

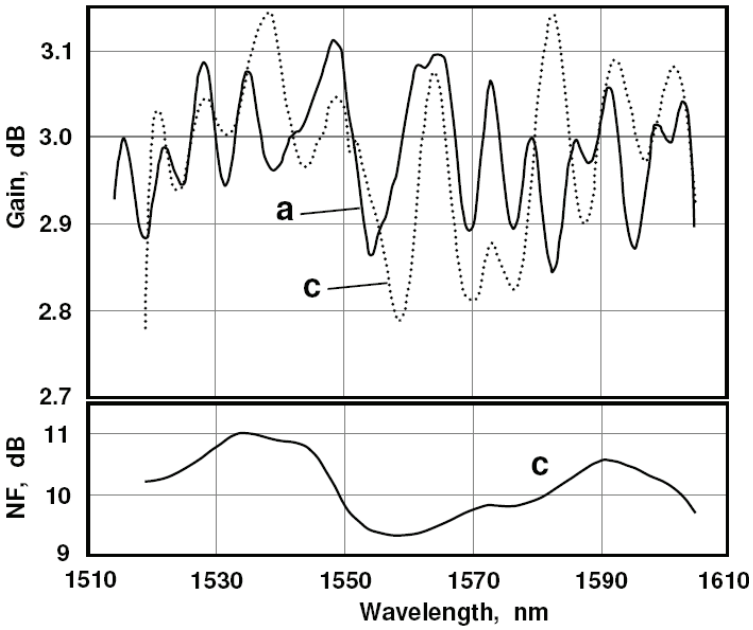

Fig. 7. Gain (top) and noise figure (bottom) spectra for a 10 km DCF Raman amplifier plus GEFs. Curve a: small launched signals and the corresponding GEF. Curves c: saturating signals with readjusted pump powers and the corresponding GEF. The pump powers are stated in Table 1 and the filter designs are illustrated in Fig. 6.

An ideal gain profile would be a horizontal line at the 3 dB baseline over a wide range. Accordingly, we now turn to the inclusion of a GEF with this aim, as described in Section 4. We have designed filters for two cases, bearing in mind that the profile to be flattened

depends upon the pumping and saturation details. We constrained each SiO_2 layer to be no thinner than 10 nm. The film structures that we obtained are depicted, with statements of their total stack thicknesses and numbers of needles, in Figs. 6 (top) for small signal operation and in Fig. 6 (bottom) for saturating signals with readjusted pumps. Some of the layers are very fine and are not easily illustrated.

Net gain and noise figure spectra with the GEFs included are presented in Fig. 7. Gain Curve a is for small signal operation with the small-signal optimised filter (top structure on Fig. 6), whereas gain Curve c is for saturated operation with pump power readjustment and its corresponding filter (lower structure on Fig. 6). The peak-to-peak ripples on Fig. 7 are 0.29 dB and 0.37 dB for Curves a and c, respectively. These values compare well to reported results using a larger number of pumps but no GEF (Namiki et al., 2001; Giltrelli et al., 2004; Cui et al., 2004). The NF curve in Fig. 7 is for saturated operation with the corresponding filter included, as determined by the Friis formula (Equation (5) with a passive element that follows the gain). The result differs little from Curve c of Fig. 5, which is not surprising; losses that come after the gain region in a compound amplifier exert negligible influence on its total noise figure.

We set the NF values on Fig. 7 in context by comparing them with what can be achieved using one C-band EDFA with saturating channels. We assume that the lowest loss of a passive 10 km DCF module (including one splice between non-identical fibres) is 5.5 dB and that the NF for a good gain-saturated commercial EDFA that follows it is 6.5 dB. Thus, the NF for the DCF+EDFA combination is 12 dB at best. Alternatively, by bringing the gain forward into the DCF via Raman amplification, Fig. 7 shows that NF_{total}, which includes the GEF and other passive components, is never worse than 11 dB. A Raman-pumped DCF with a thin film GEF therefore provides better noise performance than the combined DCF+EDFA unit, doing so across a gain bandwidth that is more than twice as wide.

6. Different channel numbers with one passive GEF

Several questions remain to assess the suitability of thin film GEFs and we now address two of them. The first follows from the variability of the Raman gain profile according to the degree of gain saturation and the associated pump powers. Does a static GEF that is optimised for amplifiers with a certain number of saturating channels remain useful when the system capacity is augmented by adding more channels? Our second question is: Is the final gain flattening tolerant to manufacture thickness errors in the thin film filters?

We started by simulating a DCRA without GEFs. As before, the pumps were backward propagating with wavelengths λ_{p1} = 1435 nm and λ_{p2} = 1485 nm but the fibre length was 11.43 km. In every case the channel powers were –3 dBm and they all lay on ITU-T grid lines. We chose the pump powers so that the internal losses of the DCF were compensated and, as before, there was an additional margin of at least 3 dB over its operating range to accommodate losses of any additional passive components.

Various channel wavelength plans can be used according to the evolution of capacity demand but we simulated a simple one in which the overall bandwidth is constant and the inter-channel spacing is reduced. Figure 8 shows gain and noise figure spectra for 30, 40, 60 and 120 launched channels. In each case we adjusted the pump powers to ensure a gain profile with two equal peaks and a baseline of 3 dB. It is clear that the gain excursion increases with the number of channels (and the associated pump power adjustment). There is also a slight migration of the operating band at the 3 dB baseline to longer wavelengths,

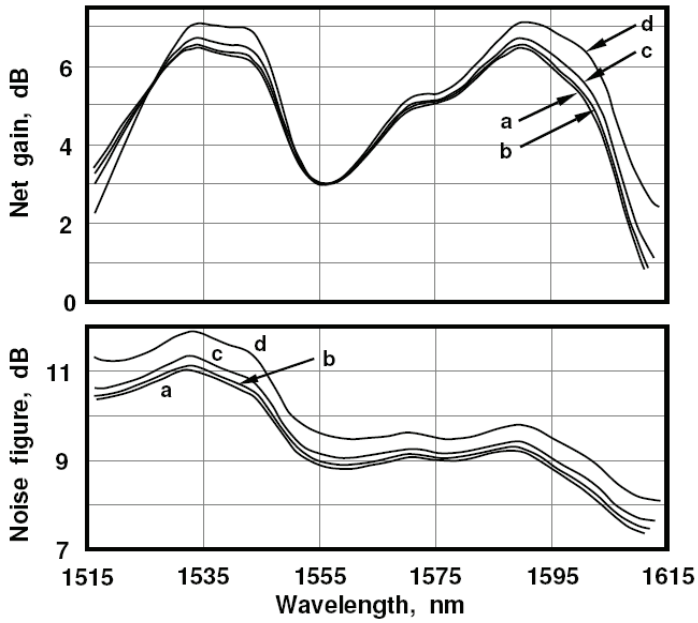

Fig. 8. Spectral variation of gain (top) and noise figure (bottom) for a 11.43 km DCF fibre Raman amplifier. The number and channel spacings are (a) 30 channels at 400 GHz, (b) 40 channels at 300 GHz, (c) 60 channels at 200 GHz and (d) 120 channels at 100 GHz. The corresponding launched pump powers at 1435 and 1485 nm are (a) 232.9 and 97.8 mW, (b) 250.5 and 101.7 mW, (c) 288.3 and 109.0 mW and (d) 410.5 and 133.1 mW.

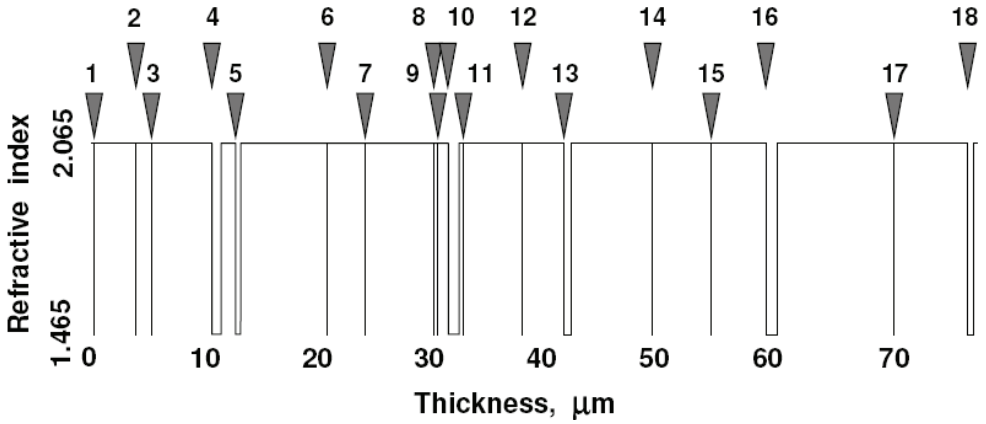

Fig. 9. The thin film design for gain equalization when operating with 60 channels spaced at 200 GHz intervals (corresponding to Curves c of Fig. 8). The arrows indicate the start positions of the eighteen SiO_2 layers.

owing to the asymmetric Raman gain profile of silica-germania glass. The noise figure curves of Fig. 8 exhibit slightly degraded performance with increasing channel numbers, and hence greater pump depletion, at shorter length coordinates within the gain medium.

We have synthesised another thin-film GEF design using the needle method, the details of which are shown in Fig. 9 (in a different pictorial format). In searching for solutions we accepted a sub-optimal film stack. Raman amplifiers exhibit a diversity of gain profiles and we aimed for simple but versatile structures. The filter was targeted at operation with 60 channels, each of –3 dBm launched power and 200 GHz spacing, in which the pumps were selected to ensure a gain profile as in Curve c of Fig. 8. Our filter design procedure predicted 18 SiO_2 layers in a Ta_2O_5 stack. The total stack thickness was 78 μm and we constrained each layer to be no thinner than 10 nm.

Figure 10 depicts the gain spectra when the GEF is included. When 60 channels of 200 GHz spacing are launched, the GEF operates according to its design criteria and the resulting peak-to-peak gain ripple is 0.30 dB over the range 1517 – 1607 nm. If there are only 30 channels with 400 GHz spacing, the filter no longer satisfies its ideal design condition and the peak-to-peak ripple is 0.38 dB within the range 1520 – 1599 nm. This small sacrifice in flattening and bandwidth is tolerable in many situations. Alternatively, if the channel density is increased above the GEF design target to 100 GHz spacing, there is a greater deterioration in performance and the peak-to-peak ripple is 0.55 dB within the range 1524 – 1596 nm. Nevertheless, such performance can be acceptable when the signals pass through only a small number of amplifying stages.

As argued in Section 3, a loss element that is located after a gain medium exerts little influence on the total noise figure. We have computed the noise figures for the whole assembly (in which the GEF is the one in Fig. 9) using the Friis cascade formula of Equation (5) and found that the resulting curves always lie within 0.15 dB of their counterparts in the bottom graph of Fig. 8.

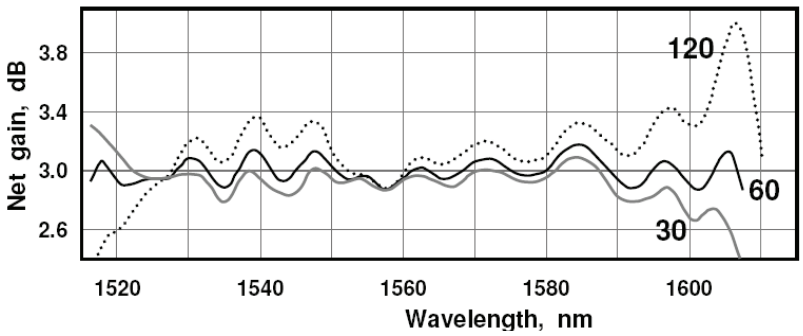

Fig. 10. Spectral variation of gain when the GEF design in Fig. 9 is placed after the DCF. The channel number and spacing are 30 channels at 400 GHz, 60 channels at 200 GHz and 120 channels at 100 GHz. The launched pump powers are as in Fig. 8.

Errors in film thickness during fabrication lead to filters with spectral characteristics that differ from their design target and so cause a deterioration in the amplifier's gain flatness. The errors can be in the form of relative or absolute film thicknesses (Thelen et al., 2002). We have applied a random number generator to simulate relative and absolute errors of 0.25% and 1.5 nm, respectively in the layers of the filter depicted in Fig. 9. (These values

significantly exceed the ones reported in Verly et al., 2002 and Thelen et al., 2002.) In this way we have simulated 100 fabricated filters for each of the two types of errors and we then selected the *worst* of each batch. Figure 11 shows the gain variation with the application of the two worst filters in which 60 channels were launched and it can be seen that the peak-to-peak gain ripples increase to 0.37 and 0.39 dB for the relative and absolute errors, respectively. Such values are tolerable in many applications.

In this section we have shown that, when there is freedom to readjust the launched pump powers, a filter that is designed for use with a certain number of saturating signals can still be applicable as the network is upgraded by adding channels. We have also studied the influence of film thickness fabrication errors on gain flattening and demonstrated that the performance of our sub-optimal GEF designs remains viable even with reasonably large error values.

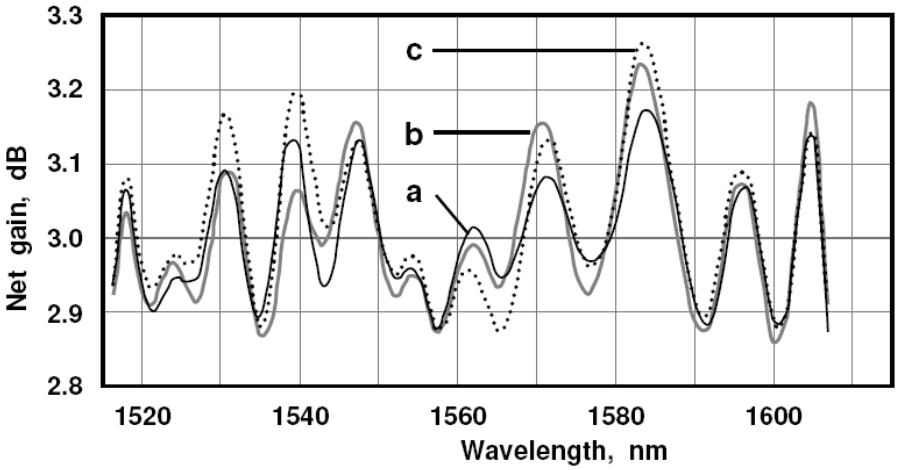

Fig. 11. Gain equalised profile for 60 channels spaced at 200 GHz: (a) no fabrication errors, (b) relative film thickness errors of 0.25%, (c) absolute film thickness errors of 0.15 nm.

7. Variation of base-line gain with one static GEF

During their operational lifetime, optical networks are often upgraded and repaired, leading to revised optical power budgets. The re-routing of cables, re-assignment of channels and inclusion of new components are common and the amplifiers in the network should ideally be sufficiently flexible to accommodate such changes without replacement. To this end, we now consider whether a DCRA can continue to provide spectrally flat performance with a new baseline gain, without having to change its GEF.

First, we modelled an 8 km DCF-based discrete Raman amplifier without a GEF. There were two backward propagating pumps (λ_{p1} = 1440 nm and λ_{p2} = 1490 nm) and 116 channels lying on ITU grid lines with 100 GHz spacing were launched, each with a power of –4 dBm. The results are presented in Fig. 12. As before, the pump powers were adjusted to provide a gain profile with two equal peaks and a local minimum between them. The local minima are at 3, 4, 5, 6 and 7 dB and so they define a sequence of baseline gains. All of the curves are very similar in shape, but the gain excursions increase slightly from bottom to top; the highest being 4.97 dB when the baseline is at 7 dB.

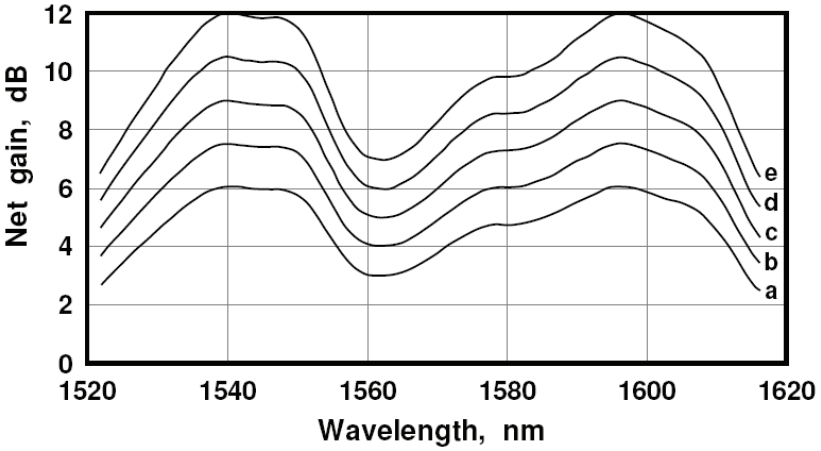

Fig. 12. Input-output gain as a function of wavelength for the following launched pump powers, P (λ_{p1}), P (λ_{p2}) in mW: (a) 281.7 and 120.5; (b) 356.3 and 142.0; (c) 448.5 and 166.1; (d) 565.4 and 194.1; (e) 716.3 and 227.8. The DCF length is 8 km.

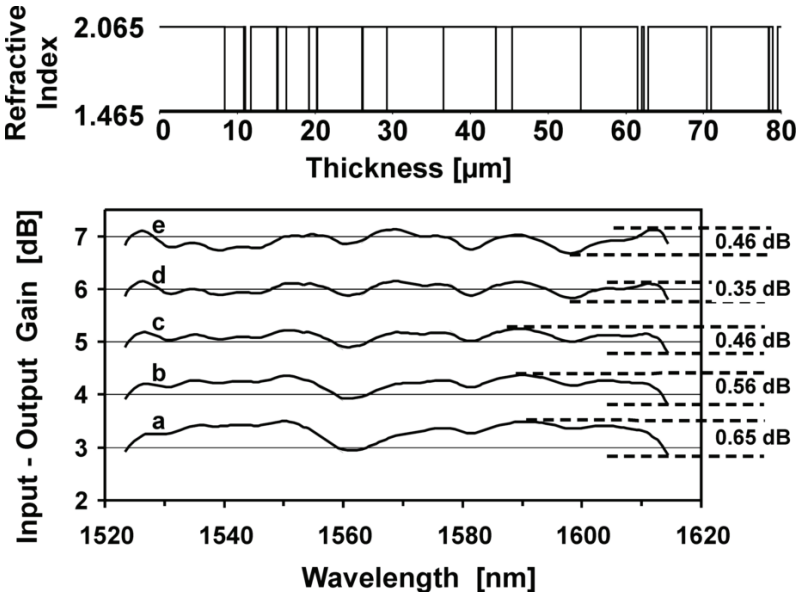

Fig. 13. Top: Thin film filter design to achieve spectral equalization of the amplifier gain Curve d of Fig. 12. Bottom: Spectral gain variations when the filter is applied. The peak-to-peak gain ripples are marked on the right. For curves a to e, the pump powers are the same as the corresponding curves in Fig. 12.

We have designed a GEF to flatten Curve d of Fig. 12 (where the baseline gain is 6 dB). Our aim was to apply it to all of the curves and compare how well it performs. The top of Fig. 13 shows its film structure, which is 18 SiO_2 layers in a Ta_2O_5 stack, with a total thickness of 80

μm. When this GEF is included in the amplifier, we obtained the gain profiles depicted in the lower part of Fig. 13. The curves are similar to each other, in which the quoted peak-to-peak gain ripples apply across the entire range of 1523 to 1614 nm. Clearly, the best flattening is achieved when the GEF was applied to the gain profile for which it was designed but acceptable performance is evident from other curves. The importance of Fig. 13 is that, provided the pump powers can be readjusted appropriately, the static GEF need not necessarily be replaced if ever the baseline gain must be varied in response to changing network operating requirements.

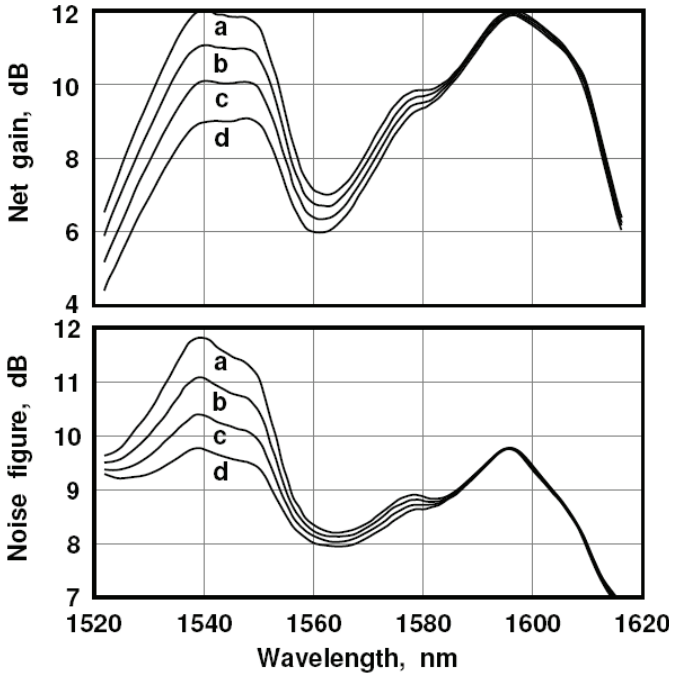

Fig. 14. Top: Gain variation with wavelength, Bottom: Noise figure variation with wavelength. Launched pump powers, $P(\lambda_{p1})$, $P(\lambda_{p2})$ in mW: (a) 716.3 and 227.8; (b) 642.0 and 241.0; (c) 569.5 and 255.1; (d) 496.5 and 271.8. Other amplifier characteristics are as in Fig. 12.

8. Reduction of the noise figure

The results in Sections 5 – 7 were mainly about the quality of gain spectral uniformity; achieving low noise figures was a secondary concern. Although we argued in Section 5 that our amplification strategy compares favourably with the use of an EDFA located after a passive span of DCF, further improvements are desirable. In particular, Figs. 5 and 8 both show two unwanted features in the noise figure spectrum: (i) performance is worst at short wavelengths because of the thermal dependence of ASE, as stated in Equation (3), and (ii) two peaks appear in saturated operation, owing to Rayleigh backscattering. Some WDM channels might therefore fail to meet the network's bit error rate requirements (Urquhart, 2008). In this section we show that, by the appropriate adjustment of the two pumps and

synthesising a filter to match, the noise figures can be improved without unacceptably deteriorating the amplifier's performance in other respects.

Gain and noise figure profiles are plotted in Fig. 14, in which the fibre span, pump wavelengths and channel input powers and spacing remain as in Section 7. The top curve on each graph (designated "a") corresponds directly to Curve e on Fig. 12, where the launched pump powers ensure a baseline gain of 7 dB and equal gain peaks. Curve a of the bottom plot of Fig. 14 shows that the corresponding noise figure spectrum has a main peak of 11.8 dB at 1539 nm and a secondary peak of 9.7 dB at 1596 nm.

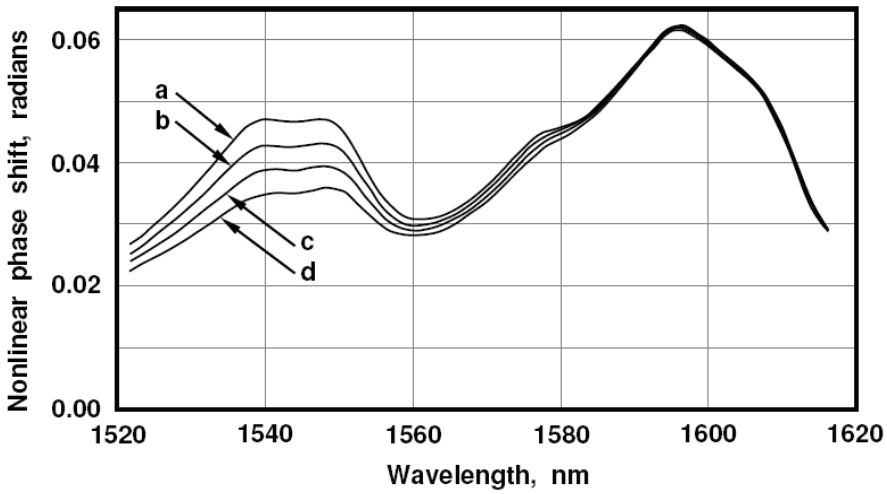

Fig. 15. Variation of nonlinear phase shift with wavelength. All of the pump powers and fibre characteristics are as in Fig. 14.

In Curves b, c and d of Fig. 14, we relaxed our previous requirement that there be two identical gain maxima and a baseline at 7 dB. Instead, we concentrated on the noise figure spectrum with the aim of selecting pump powers that progressively suppress the peak at 1538 nm to achieve better uniformity. In Curve d the chosen pump powers ensure that the two noise figure peaks are equal, having a value of 9.7 dB, which is clearly beneficial for the shorter wavelength channels. The method used was to reduce the power at λ_{p1} and increase it at λ_{p2}. When this was done, there was a significant reduction of the signal DRB near the short wavelength gain peak and a slight lowering of the ASE at all shorter signal wavelengths. The pump-to-pump SRS was also reduced and so the power at λ_{p2} had to be increased to compensate and thus achieve a revised baseline gain of 6 dB. However, as Curve d in the upper plot of Fig. 14 shows, there was a corresponding loss of symmetry in the gain profile and the question is: does it matter?

One possible concern is that an asymmetrical gain profile might provoke unacceptable nonlinear cross-talk within the DCF at the longer signal wavelengths. According to Equation (6), nonlinear phase shift is proportional to the integral of the signal powers over the fibre length coordinate. We need to ensure that it is not intolerably enhanced by varying the ratio of pump powers to achieve an asymmetric gain profile. Figure 15 is a plot of the nonlinear phase shift. It displays two peaks that are associated with the gain peaks on Fig. 14 because

the path averaged signal power is high when the gain is high. Curves b, c and d of Fig. 15 show that by progressively changing the ratio of powers at λ_{p1} and λ_{p2} the short wavelength peak is depressed but the long wavelength peak is largely unaffected. In Curve a much of the long wavelength gain results from the guided wave at λ_{p2} being amplified by that at λ_{p1}. Lowering the power at λ_{p1} reduces the Raman pump-to-pump interaction. Therefore, pump-to-pump interactions are less important contributors in the other curves, where the launched power at λ_{p2} is increased in a manner that compensates for the effect.

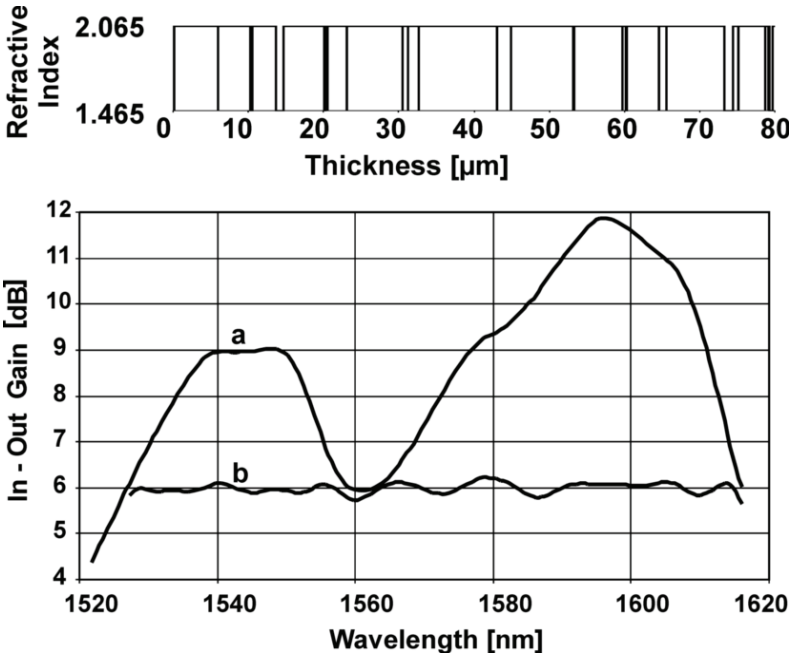

Fig. 16. Top: Thin film filter design (with 23 SiO_2 layers) to achieve spectral equalisation of the gain Curve d of Fig. 14. Bottom: The spectral gain variation before (Curve a) and after (Curve b) the filter is applied.

We have synthesised a GEF design to equalise the distorted gain profile (Curve d of Fig. 14). Figure 16 shows the result after applying the filter to the amplifier, together with the target function for which it was designed; a peak-to-peak gain ripple of 0.49 dB over the range 1527–1615 nm was achieved. The performance should be compared with that of Curve d of Fig. 13, where the baseline gain is also 6 dB. The 0.49 dB ripple in Fig. 16 is slightly worse but it is an acceptable value for intermediate haul DWDM systems.

In summary, when the pump powers are adjusted to obtain tilted gains, the noise figure and the nonlinear phase shift are both reduced at shorter wavelengths but there is no decrease of the nonlinear phase shift at longer signal wavelengths. We have designed a GEF to compensate for the asymmetric profile, providing acceptably uniform amplification across a wider spectrum than a combined C- and L-band EDFA. Pumping to achieve improvements in the short wavelength noise figures at the expense of an asymmetric gain profile is therefore beneficial.

9. Conclusion

We have presented simulations of a spectral equalisation strategy for dispersion compensating fibre Raman amplifiers. Flat and broad bandwidth gain profiles can be obtained by launching only two contra-directional pumps into dispersion compensating fibre (DCF) and following it with a gain equalisation filter (GEF) based on dielectric thin film technology. To this end, we have optimised such filters using a trusted technique called the needle method. When a GEF is included, the amplifier can provide good gain profile uniformities for over 100 channels in both small signal and gain saturation.

The strategy explained in this chapter is versatile, which is partly because our filters were "sub-optimal", meaning that we avoided highly refined design solutions that perform well only within specific circumstances. For example, sub-optimal film structures can provide good spectral equalisation even when imperfect fabrication causes thickness errors. Moreover, by retaining the flexibility to adjust the two launched pump powers, the spectral flatness continues to be acceptable in revised operating conditions, without necessarily having to change the GEF. In particular, we have shown that the amplifier performance remains viable when the number of channels is increased or when the baseline gain must be varied to accommodate new demands of the optical network.

The total noise figure of the amplifier is least when the GEF is placed after the DCF gain medium, as we have done. Moreover, it is possible to achieve further improvements to the noise performance by pumping for tilted (asymmetric) gains and designing a GEF for such operation to obtain good profile uniformity. We have argued that this approach can be used without incurring unacceptable additional nonlinear crosstalk.

The gain equalisation strategy that we describe in this chapter uses passive filters, which are low cost, high reliability components of low thermal sensitivity. Moreover, with only two pump lasers to manage, it reduces the demands on the control software, and hence network management, and we have derived an approximate analytical model to illustrate this feature. Application can be in cost-sensitive but high capacity systems where the signals pass through a cascade of dispersion-compensating amplifier stages.

10. Acknowledgement

Guido Boyen and André Brückmann each received an EU Erasmus scholarship. Project funding was by Spanish Ministry of Education and Science project TEC2010-20224-C02-01.

11. Appendix: Approximate analytical model of dual-wavelength pumping

We present a theory to predict the dual-wavelength pumped gain spectrum when the channels are contra-directional and low power. For ease of calculation, we assume that the two pumps are launched at z = 0. Their mutual interaction is described by:

$$\frac{dP_{p1}}{dz} = -\Lambda\,\Gamma_{12}\,P_{p1}\,P_{p2} - \alpha_p\,P_{p1} \tag{8}$$

$$\frac{dP_{p2}}{dz} = +\Gamma_{12}\,P_{p1}\,P_{p2} - \alpha_p\,P_{p2}\ , \tag{9}$$

where $\Lambda = \lambda_{p2}/\lambda_{p1}$ and the losses are assumed equal ($\alpha_{p1} = \alpha_{p2} = \alpha_p$). Equations (8) and (9) include saturation by transfer of power from one pump to the other with gain coefficient Γ_{12}

from Equation (1). However, they do not account for ASE or depletion by the propagating signal(s). They yield analytical solutions and to do this we transform the coordinates by defining the power ratio $R(z) = P_{p1}/P_{p2}$ and the weighted sum $S(z) = (P_{p1} + \Lambda P_{p2})$, giving:

$$\frac{dS}{dz} = -\alpha_p S \tag{10}$$

$$\frac{dR}{dz} = -\Gamma_{12} R S \cdot \tag{11}$$

The initial conditions are $S(z = 0) = S_0 = [P_{p1}(0) + \Lambda P_{p2}(0)]$ and $R(z = 0) = R_0 = P_{p1}(0)/P_{p2}(0)$. Equations (10) and (11) are then easily solved to provide:

$$S(L) = S_0 \exp(-\alpha_p L) \tag{12}$$

$$R(L) = R_0 \exp(-\Gamma_{12} S_0 L_{eff}) . \tag{13}$$

L_{eff} is identified as the effective length term, which is commonly used in Raman amplifier theory: $L_{eff} = [1 - \exp(-\alpha_p L)]/\alpha_p$. When necessary, Equations (12) and (13) are easily converted back to power coordinates using $P_{p1} = SR/(R + \Lambda)$ and $P_{p2} = S/(R + \Lambda)$.

We now introduce a propagating signal of tuneable wavelength λ_s and we assume that it is not sufficiently powerful to deplete the pumps. The signal is contra-directional and therefore it is launched at $z = L$ with power P_{in}. The fibre loss at the signal wavelength is α_s and in general $\alpha_s \neq \alpha_p$. We also require the Raman gain coefficients for the pump-signal interactions, Γ_{1s} and Γ_{2s}, defined in Equation (1).

When the signal is included, we have three differential equations describing the optical powers propagating in the fibre. The first two are Equations (8) and (9), without any modifications and subject to the same boundary conditions as before. The third one is

$$\frac{dP_s}{dz} = -\Gamma_{1s} P_{p1} P_s - \Gamma_{2s} P_{p2} P_s + \alpha_s P_s \tag{14}$$

Equation (14) can be solved using the previous quantities R(z) and S(z). There are three terms on the right hand side to be integrated. The first one can be transformed using R and S, together with Equation (11):

$$\begin{aligned} \int_{z' = L}^{z} P_{p1}(z')\,dz' &= \int_{z' = L}^{z} \frac{S(z')R(z')}{(R(z') + \Lambda)} . dz' \\ &= -\left(\frac{1}{\Gamma_{12}}\right) \int_{z' = L}^{z} \frac{d\,R(z')/dz'}{(R(z') + \Lambda)} . dz' = -\left(\frac{1}{\Gamma_{12}}\right) . \ln\left(\frac{R(z) + \Lambda}{R(L) + \Lambda}\right) \end{aligned} \tag{15}$$

The second term on the right of Equation (14) can be integrated with the aid of another defined real variable, I(z), which is the inverse of R(z): $I(z) = 1/R(z)$. In this way, an alternative statement of Equation (11) is $dI/dz = +\Gamma_{12} S I$. Then, the second integration becomes:

$$\begin{aligned} \int_{z' = L}^{z} P_{p2}(z')\,dz' &= \int_{z' = L}^{z} \frac{S(z')I(z')}{(1 + \Lambda I(z'))} . dz' = \left(\frac{1}{\Gamma_{12}}\right) \int_{z' = L}^{z} \frac{d\,I(z')/dz'}{(1 + \Lambda I(z'))} . dz' \\ &= \left(\frac{1}{\Lambda \Gamma_{12}}\right) . \ln\left(\frac{1 + \Lambda / R(z)}{1 + \Lambda / R(L)}\right) \end{aligned} \tag{16}$$

The third integration from the right of Equation (14) is merely a loss term.
By combining all three integrations, Equation (14) can be solved to give the length-dependence of the signal power and thus the net (input-output) amplifier gain:

$$G_{net} = \frac{P_s(z=0,\lambda_s)}{P_{in}} = \left(\frac{R_0 + \Lambda}{R(L) + \Lambda}\right)^{\frac{\Gamma_{1s}(\lambda_s)}{\Gamma_{12}}} \cdot \left(\frac{1 + \Lambda/R(L)}{1 + \Lambda/R_0}\right)^{\frac{\Gamma_{2s}(\lambda_s)}{\Lambda\Gamma_{12}}} \cdot \exp[-\alpha_s L], \quad (17)$$

where the wavelength dependence is provided through the terms $\Gamma_{1s}(\lambda)$ and $\Gamma_{2s}(\lambda)$. (In general, α_p and α_s also vary with wavelength.) Equation (13) allows us to determine R(L) as a function of the inputs S_0 and R_0. Owing to our choice of length coordinate, the amplified signal exits the fibre at $z = 0$. However, $P_{p1}(0)$ and $P_{p2}(0)$ are known values and G_{net} is a relation between input and output signal powers, which applies irrespective of the point of launch, provided that it is opposite that of the pumps.
Equation (17) is plotted for some typical small signal operating conditions in Fig. 17, where the DCF is the same as in Fig. 4. The pump wavelength separation is 30, 40 and 50 nm in Curves a, b and c, respectively, so as to provide ever wider operating profiles. All of the pump powers, which are specified in Table 2, were selected for a baseline gain of 3 dB and two peaks of equal magnitude. Curve c is, in fact, two sets of points, which largely overlap. The solid line was plotted from Equation (17) by scanning λ_s across a range; the dotted line is merely a reproduction of Curve a from Fig. 4, which was obtained by numerical solution of Equation (2) with 151 simultaneous low power launched signals.
The two sets of points that constitute Curve c are very close but Table 2 reveals that slightly different pump powers were required. (However, the total power, $[P(\lambda_{p1}) + P(\lambda_{p2})]$, is the same within computational error.) We attribute the small difference to two effects: (i) the absence of ASE and (to a lesser extent) RBS from the analytical model and (ii) our assumption of equal pump losses ($\alpha_{p1} = \alpha_{p2} = \alpha_p$). Although the launched signals might be very small, the spontaneous scattering is amplified bi-directionally, causing some depletion of the pumps. Moreover, the choice of α_p is a compromise that becomes less satisfactory as the wavelength difference ($\lambda_{p2} - \lambda_{p1}$) is increased. Nevertheless, the strong correlation between the two sets of points in Curve c indicates that the analytical model can provide a good approximation to the required pump powers and a physical insight into the gain mechanism in the small signal limit. It can thus be used to establish initial performance estimates prior to finding accurate numerical solutions.

Curve	λ_{p1} & λ_{p2}, nm	$P(\lambda_{p1})$, mW	$P(\lambda_{p2})$, mW	Bandwidth at baseline, nm	Excursion, dB
a	1445 & 1475	79.6	86.9	41.6	0.6
b	1440 & 1480	118.9	94.3	71.0	1.6
c (solid)	1435 & 1485	160.8	101.5	92.4 ± 0.5	2.9 ± 0.05
c (dotted)		173.3	89.1		

Table 2. Data for plotting Fig. 17 and the resulting bandwidths and gain excursions.

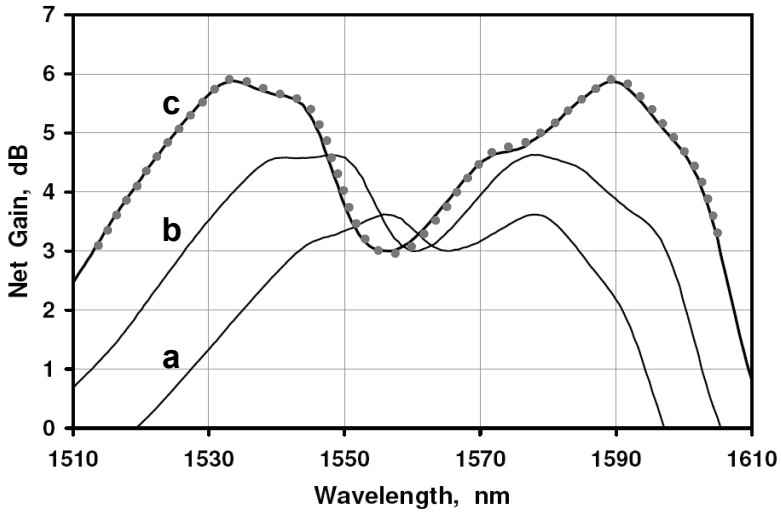

Fig. 17. Spectral gain variation with two pump wavelengths. Fibre length is 10 km and the pump loss coefficient α_p is the average of $\alpha(\lambda_{p1})$ and $\alpha(\lambda_{p2})$. Other data are in Table 2.

12. References

G.P. Agrawal (2005), Theory of Fibre Amplifiers, Chapter 2 in *Raman Amplification in Fiber Optical Communication Systems*, C. Headly and G.P. Agrawal (Editors), Academic Press, ISBN 978-0-120445066.

A. Boskovic, S.V. Chernikov, J.R. Taylor, L. Grüner-Nielsen, O.A. Levring (1996), Direct Continuous-Wave Measurement of n_2 in Various Types of Telecommunication Fiber at 1.55 μm, *Optics Letters*, 21 (24), 1966-1968.

J. Bromage (2004), Raman Amplification for Fiber Communications Systems, *IEEE Journal of Lightwave Technology*, 22 (1), 79–93.

J. Bromage, P.J. Winzer, R.-J. Essiambre (2004) Multiple Path Interference and its Impact on System Design, Chapter 15 in M.N. Islam (Ed.), *Raman Amplifiers for Telecommunications 2: Sub-Systems and Systems*, Springer. ISBN 978-0387406565.

S. Cui, J. Liu, X. Ma (2004), A Novel Efficient Optimal Design Method for Gain-Flattened Multiwavelength Pumped Fiber Raman Amplifier, *IEEE Photonics Technology Letters*, 16 (11), 2451–2453.

E. Desurvire (1994) Erbium Doped Fiber Amplifiers: Principles and Applications, Wiley. ISBN 978-0471266273.

M. Giltrelli, M. Santagiustina (2004), Semianalytical Approach to the Gain Ripple Minimization in Multiple Pump Fiber Raman Amplifiers, *IEEE Photonics Technology Letters*, 16 (11), 2454–2456.

L. Grüner-Nielsen, Y. Qian, P.B. Gaarde (2006), Dispersion Compensating Fibers For Raman Applications, *Journal of Optical Fiber Communications*, 3, 61-89.

ITU-T Recommendation G.694.1 (2002-06), Spectral Grids for WDM Applications: DWDM Frequency Grid, available from www.itu.int/rec/T-REC-G.694.1-200206-I.

M.N. Islam, C. DeWilde, A. Kuditcher (2004), Wideband Raman Amplifiers, Chapter 14 in *Raman Amplifiers for Telecommunications*, Vol. 2, M.N. Islam (Editor), Springer, ISBN 978-0-387406565.

S. Jiang, B. Bristiel, Y. Jaouen, P. Gallion, E. Pincemin (2007a), Bit-Error-Rate Evaluation of the Distributed Raman Amplified Transmission Systems in the Presence of Double Rayleigh Backscattering Noise, *IEEE Photonics Technology Letters*, 19 (7), 468-470.

S. Jiang, B. Bristiel, Y. Jaouen, P. Gallion, E. Pincemin, S. Capouilliet (2007b), Full Characterisation of Modern Transmission Fibers for Raman-Amplified Communication Systems, *Optics Express*, 15 (8), 4883-4892.

F. Koch, S.A.E. Lewis, S.V. Chernikov, J.R. Taylor, V. Grubsky, D.S. Starodubov (2000), Broadband Gain Flattened Raman Amplifier to Extend Operation in the Third Telecommunication Window, Proceedings, *Conference on Optical Fiber Communications*, paper FF-3, ISBN 978-0780359529.

S.A.E. Lewis, S.V. Chernikov, J.R. Taylor (1999), Temperature-Dependent Gain and Noise in Fiber Raman Amplifiers, *Optics Letters*, 24 (24), 1823-1825.

H.A. Macleod (2010), *Thin Film Optical Filters*, 4th Edition, CRC Press, see especially Chapters 2 and 3, ISBN 978-1420073027.

T. Miyamoto, T. Tsuzaki, T. Okuno, M. Kakui, M. Hirano, M. Onishi, M. Shigematsu (2002), Raman Amplification over 100-nm Bandwidth with Dispersion and Dispersion Slope Compensation for Conventional Single Mode Fiber, *Conference on Optical Fiber Communications*, Anaheim, USA, Paper TuJ7, ISBN 1-55752-701-6.

S. Namiki, Y. Emori, (2001), Ultrabroad-band Raman Amplifiers Pumped and Gain-Equalized by Wavelength-Division-Multiplexed High-Power Laser Diodes, *IEEE Journal of Selected Topics in Quantum Electronics*, 7 (1), 3–16.

S. Namiki, Y. Emori, A. Oguri (2005), Discrete Raman Amplifiers, Chapter 4 in *Raman Amplification in Fiber Optical Communication Systems*, C. Headley, G.P. Agrawal (Editors), Elsevier Academic Press, ISBN 978-0-120445066.

S. Namiki, N. Tsukiji, Y. Emori (2004), Pump Laser Diodes and WDM Pumping, Chapter 5 of M.N. Islam, *Raman Amplifiers for Telecommunications 1: Physical Principles*, M.N. Islam (Editor), Springer, New York. ISBN 978-0-387007519.

B. Neto, C. Reis, A. Teixeira, P.S. Andre, N. Wada (2009), proceedings, *SBMO/IEEE Microwave and Optoelectronics Conference*, Boston USA, 687-689. ISBN 978-1-4244-5356-6.

B.T. Sullivan, J.A. Dobrowolski (1996), Implementation of a Numerical Needle Method for Thin-Film Design, *Applied Optics*, 35 (28), 5484-5492.

H. Takashashi (1995), Temperature Stability of Thin-Film Narrow Bandpass Filters Produced by Ion-Assisted Deposition, *Applied Optics*, 34 (4), 667-675.

A. Thelen, M. Tilsch, A.V. Tikhonravov, M.K. Trubetskov, U. Brauneck (2002), Topical Meeting on Optical Interference Coatings (OIC 2001): Design Contest Results, *Applied Optics*, 41 (16), 3022-3038.

A.V. Tikhonravov, M.K. Trubetskov, G.W. DeBell (1996), Application of the Needle Optimization Technique to the Design of Optical Coatings, *Applied Optics*, 35 (28), 5493–5508.

P. Urquhart (2008), Optical Fiber Transmission, Chapter 6 in G. Hill (editor), *The Cable and Telecommunications Professionals' Reference* Vol. 2, 3rd Ed., Focal Press, ISBN 978-0-240-80748-5.

P. Urquhart, O. García López, G. Boyen, A. Brückmann (2007), Optical Amplifiers for Telecommunications, Proceedings, *IEEE Symposium on Intelligent Signal Processing, WISP 2007*, Alcala de Henares, 3-5 October 2007, ISBN 978-1-4244-0830-6.

P.G. Verly (2002), Design of a Robust Thin-Film Interference Filter for Erbium-Doped Fiber Amplifier Gain Equalization, *Applied Optics*, 41 (16), 3092–3096.

X. Zhou, M. Feuer, M. Birk (2006), A Simple Feed-Forward Control Algorithm for Fast Dynamic Gain Profile Control in a Multi-Wavelength Forward Pumped Fibre Raman Amplifier, *IEEE Photonics Technology Letters*, 18 (9), 1004-1006.

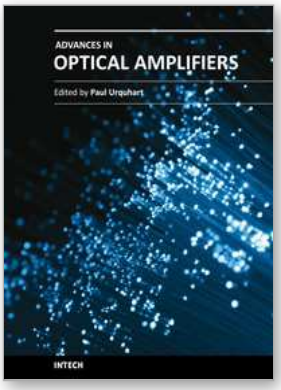

Advances in Optical Amplifiers
Edited by Prof. Paul Urquhart

ISBN 978-953-307-186-2
Hard cover, 436 pages
Publisher InTech
Published online 14, February, 2011
Published in print edition February, 2011

Optical amplifiers play a central role in all categories of fibre communications systems and networks. By compensating for the losses exerted by the transmission medium and the components through which the signals pass, they reduce the need for expensive and slow optical-electrical-optical conversion. The photonic gain media, which are normally based on glass- or semiconductor-based waveguides, can amplify many high speed wavelength division multiplexed channels simultaneously. Recent research has also concentrated on wavelength conversion, switching, demultiplexing in the time domain and other enhanced functions. Advances in Optical Amplifiers presents up to date results on amplifier performance, along with explanations of their relevance, from leading researchers in the field. Its chapters cover amplifiers based on rare earth doped fibres and waveguides, stimulated Raman scattering, nonlinear parametric processes and semiconductor media. Wavelength conversion and other enhanced signal processing functions are also considered in depth. This book is targeted at research, development and design engineers from teams in manufacturing industry, academia and telecommunications service operators.

How to reference
In order to correctly reference this scholarly work, feel free to copy and paste the following:

André Brückmann, Guido Boyen, Paul Urquhart, Amaia Legarrea Imízcoz, Nuria Miguel Zamora, Bruno Bristiel and Juan Mir Pieras (2011). Dual-Wavelength Pumped Dispersion-Compensating Fibre Raman Amplifiers, Advances in Optical Amplifiers, Prof. Paul Urquhart (Ed.), ISBN: 978-953-307-186-2, InTech, Available from: http://www.intechopen.com/books/advances-in-optical-amplifiers/dual-wavelength-pumped-dispersion-compensating-fibre-raman-amplifiers

INTECH
open science | open minds

InTech Europe
University Campus STeP Ri
Slavka Krautzeka 83/A
51000 Rijeka, Croatia
Phone: +385 (51) 770 447
Fax: +385 (51) 686 166
www.intechopen.com

InTech China
Unit 405, Office Block, Hotel Equatorial Shanghai
No.65, Yan An Road (West), Shanghai, 200040, China
中国上海市延安西路65号上海国际贵都大饭店办公楼405单元
Phone: +86-21-62489820
Fax: +86-21-62489821